Validation Study on Spatially Averaged Two-Fluid Model for Gas-Solid Flows: II. Application to Risers and Fluidized Beds

Simon Schneiderbauer
Christian-Doppler Laboratory for Multi-Scale Modelling of Multiphase Processes, Johannes Kepler University, Altenbergerstr. 69, Linz, Austria

Dept. of Particulate Flow Modelling, Johannes Kepler University, Altenbergerstr. 69, Linz, Austria

DOI 10.1002/aic.16141
Published online March 10, 2018 in Wiley Online Library (wileyonlinelibrary.com)

In our prior study (Schneiderbauer, AIChE J. 2017;63(8):3544–3562), a spatially averaged two-fluid model (SA-TFM) was presented, where closure models for the unresolved terms were derived. These closures require constitutive relations for the turbulent kinetic energies of the gas and solids phase as well as for the subfilter variance of the solids volume fraction. We had ascertained that the filtered model do yield nearly the same time-averaged macroscale flow behavior in bubbling fluidized beds as the underlying kinetic-theory-based two-fluid model, thus verifying the SA-TFM model approach. In the present study, a set of 3D computational simulations for validation of the SA-TFM against the experimental data on riser flow and bubbling fluidized beds is performed. Finally, the SA-TFM predictions are in fairly good agreement with experimental data in the case of Geldart A and B particles even though using very coarse grids. © 2018 The Authors AIChE Journal published by Wiley Periodicals, Inc. on behalf of American Institute of Chemical Engineers *AIChE J*, 64: 1606–1617, 2018
Keywords: cluster induced turbulence, multiphase turbulence, turbulent kinetic energy, kinetic theory based two-fluid model, coarse-grid simulations

Introduction

Granular materials have diverse industrial applications. Many of these are operated in an agitated regime of the particles to favor the contact with a fluid phase and, therefore, increase the mass and energy transfer rates. Especially, fluidized beds establish these features. During the last decades the analysis of the hydrodynamics or the efficiency of fluidized beds through numerical simulations has become increasingly common, where the two-fluid model (TFM) approach has proven to provide fairly good predictions of the hydrodynamics of gas-solid flows.[1,2] However, due to computational limitations a fully resolved simulation of industrial scale reactors is still unfeasible. It is, therefore, common to use coarse grids to reduce the demand on computational resources, which inevitably neglects small (unresolved) scales.[3] Many subgrid drag modifications have, therefore, been proposed to account for the effect of small unresolved scales on the resolved mesoscales in this case.[4–22] Our previous studies[20,21,23] reveal that the state-of-the-art subgrid drag modifications reveal different functional dependencies as well as completely different functional forms. For example, while EMMS[4] and the Kuipers relation[16] do not show a grid dependency, the other drag modifications predict a reduction of the effective drag with increasing grid/filter size. Furthermore, the Princeton group[10,19] and our group[21] ascertained a dependence of the drag modification on the filtered slip velocity. Finally, even drag modifications[10,14,17,19,20] derived from filtering fine grid simulations reveal significantly different forms, while the functional dependencies and trends seem to be quite similar. Recent studies[23,24] clearly indicate that those residual correlations obtained from filtering fine grid data considerably depend on the particle properties (size and density), the superficial gas velocity and the geometrical setup of the fine grid simulation (full fluidized bed or periodic domain), which can be explained as follows. Those filtered subgrid modifications are deduced from fine-grid TFM simulations (using grid resolutions of several particle diameters to resolve all relevant flow structures), which are filtered using filters of different sizes. Different markers such as, gas voidage and slip velocity, are then used to classify the subfilter scale state and averaged to obtain statistics of the filtered quantities. It has to be emphasized that those markers are solely guesses of the relevant functional dependencies. The choice of the markers is, however, certainly based on physical reasoning but not on a thorough mathematical derivation. Finally, subgrid modifications are directly deduced from the filtered data using curve fitting. To sum up, so far no general theory existed, which connects all of this different modifications.

In our previous study,[1] we have presented a spatially averaged two-fluid model (SA-TFM), which enables the coarse grid simulation of dense gas-solid flows. As outlined before, these averaged TFM equations require constitutive models for the residual correlations appearing due to averaging. On the one hand, the unresolved part of the gas-solid drag force is

Correspondence concerning this article should be addressed to S. Schneiderbauer at simon.schneiderbauer@jku.at.

Table 1. Case Descriptions of Riser Flow Condition[30]

Material	Case	W_g (m s^{-1})	M_s (kg s^{-1})	T (°C)	p_{out} (kPa)
Group A	1	5.14	1.44	20.5	182
	2	5.14	9.26	20.5	167
Group B	3	5.71	5.54	23	100
	4	7.58	7.03	23	102
	5	7.58	14.00	23	105

W_g Denotes the superficial gas velocity at the riser inlet, M_s the solids circulation rate, T the gas temperature and p_{out} the pressure at the riser outlet.

derived by employing a series expansion to the microscopic drag coefficient and on the other hand the Reynolds-stress like contributions are closed similar to Boussinesq-approximation in single phase flows. The subsequent averaging of this linearized drag force reveals that the unresolved part of the interphase momentum exchange is a function of the turbulent kinetic energies (TKE) of both, the gas and solid phase, and the variance of the solids volume fraction (VVF). A comparison with fine grid data proves that this approach for the drag modification is valid for a wide range of particle properties (size and density). Instead of using functional fits to relate the values of the TKEs and VVF to the local resolved mesoscale state of flow, equations for the TKEs as well as the VVF are derived,[25–28] which allow for the accurate determination of the averaged drag force.

While in our previous study[1] the SA-TFM was verified against highly resolved simulations of a bubbling fluidized bed a thorough validation for a different fluidization regime is still missing. Thus, in Part I of this article[29] we present an a-priori analysis verifying the predications of the SA-TFM closures near solid boundaries. Consequently, the SA-TFM approach is compared with experimental data in the case of gas-particle flows in risers and bubbling fluidized beds in Part II. In particular, we apply this coarse grid model to the NETL challenging problem,[30] where the flow of Geldart A and B particles in a riser section of a circulating fluidized bed is studied as well as to the bubbling fluidized bed of Zhu et al.[31] Part II is organized as follows. First, we describe the different cases studied including boundary conditions and numerical settings. Second, we discuss the result with respect to the experimental data. Finally, a conclusion ends this paper.

Case Descriptions

In the following, we verify the SA-TFM (Table 1 in Part I)[29] in the case of (i) the riser section of a Circulating Fluidized Bed,[30] and (ii) in the case of a bubbling fluidized bed of Geldart type A particles.[31] According to Part I[29] the mixing length, l_{mq} appearing in the constitutive relations for the mesoscale stresses has to be corrected near walls[32]

$$l_{mq} = C_{vq} \min\left(\Delta_f, \delta\right)$$

where Δ_f denotes the filter size or more specifically the grid spacing. Furthermore, δ denotes the cell wall distance. As in industrial applications isotropic grid spacings in each lateral direction may not be feasible (particularly in the case of risers), the filter size is assumed to be the maximum edge length of a hexahedral cell, h_{max} in the case of anisotropic meshes, that is, $\Delta_f = h_{max}$.[33,34] It has to be further stressed that the SA-TFM model coefficients (ξ_{gs}, $\xi_{\phi g}$, $\xi_{\phi s}$, C_{vg}, C_{vs}, $C_{\phi g}$, $C_{\phi s}$, $C_{\epsilon g}$, $C_{\epsilon s}$) have the same values throughout this article as given by Table 1 in Part I.[29]

Following our previous studies[2,20,21,35] we apply the CFD solver FLUENT (version 16.2) to solve the SA-TFM equations. As these equations are not covered by its standard functional range, these are, therefore, implemented by user defined functions. For the discretization of the convective terms appearing in the transport equations a second-order upwind scheme is used. The derivatives appearing in the diffusion terms are computed by a least squares method, and the pressure-velocity coupling is achieved by the SIMPLE algorithm, whereas the face pressures are computed as the average of the pressure values in the adjacent cells (linear interpolation). The time step size is set to 0.001 s, which ensures a Courant number less than 1. Initially, the riser is assumed to be empty, while the bubbling fluidized bed was initialized with the appropriate solids inventory. After an initial startup phase, the simulations reach steady state operation. Here, the total solids inventory and the pressure at the gas inflow constitute adequate monitors. Within the steady state operation we obtained the time averages for the gas pressure gradient, the solids upward velocity and the solids mass flux for at least 20 s.

As fluidized beds mostly exhibit dense regions (in risers typically core annular flows can be observed,[30] where dense particle strands form at the riser walls), the turbulent particle stresses (Table 1 in Part I[29]) are augmented by a frictional rheology.[2] These models accounts for the long enduring multiple frictional contacts in dense regions, where the solids volume fraction is close to maximum packing conditions. Here, no turbulent (cluster-like) behavior of the solid phase can be observed, as there is simply no room for those turbulent fluctuations. Thus, the SA-TFM model predicts vanishing turbulent stresses near the jamming point,[1] which was assumed to be at $\phi^{max} = 0.6$. For more details on the frictional stress model the reader is referred to Table A1 of Part I.[29] Finally, we apply the drag model proposed Wen and Yu[35] to the microscopic drag coefficient to compute the effective interphase momentum exchange in Table 1 of Part I.[29]

Riser Flow

A schematic drawing of the riser section of the Circulating Fluidized Bed (CFB) is shown in Figure 1a. The operating conditions of the riser are summarized in Table 1, were we focus on cases 2, 4, and 5 in this study. Here, the Geldart group A particles represent 59 μm glass beads and the group B particles correspond to 802 μm high density ethylene particles with a density of $\rho_s = 2425$ kg m^3 and $\rho_s = 863$ kg m^3, respectively. The density of the gas phase was assumed to behave like an ideal gas at constant temperature T. For a more detailed description of the riser section the reader is referred to Panday et al.[30] It has to be noted that at the riser walls we apply a no-slip boundary conditions for both the gas and the solid phase as no-slip boundary conditions better predict the downflow of particles in the wall region than free-slip boundary conditions. In particular, partial-slip boundary conditions[2,37–39] might be the most appropriate choice for riser flows; however, these require on the one hand a fine grid resolution near the wall and on the other hand, the evaluation of the granular temperature (microscopic fluctuations), which appears nonsignificant at the mesoscale.[1] Thus, these are not considered in the current approach.

The riser was discretized (including 1 m solid inlet pipe and 1 m exit pipe) using approximately (i) 1,60,000 hexahedral cells (coarse grid), (ii) 14,000 hexahedral cells (*very* coarse

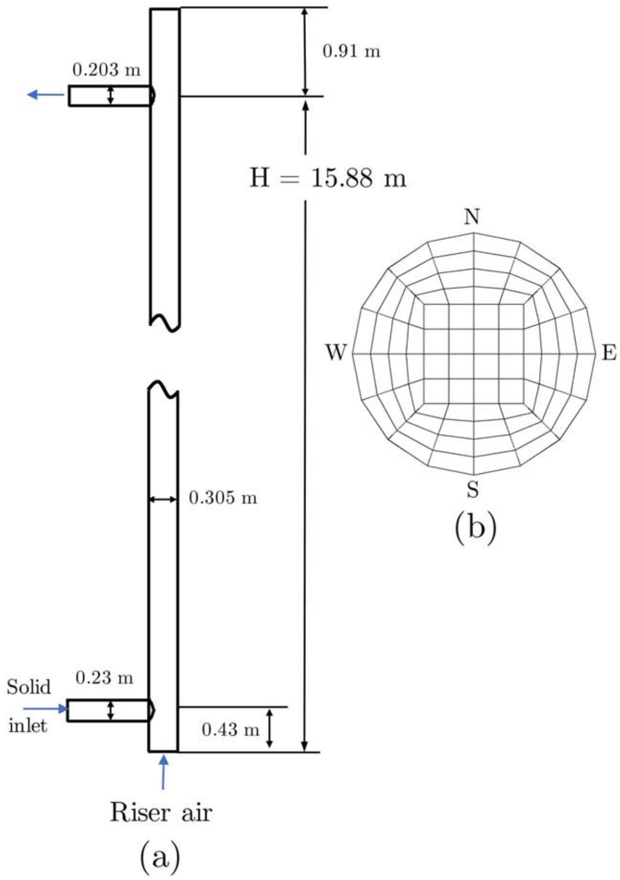

Figure 1. (a) Schematic drawing of the riser section of the Circulating Fluidized Bed challenge problem[30]; (b) Cross-sectional view of baseline grid for the very coarse grid I including azimuthal directions.

[Color figure can be viewed at wileyonlinelibrary.com]

grid I), and (iii) 6000 hexahedral cells (*very* coarse grid II). In Figure 1a cross-sectional view of the base line grid for the *very* coarse grid I is shown. Here, the horizontal grid spacing in the center of the riser is approximately 30 mm, while in the boundary layer like annular region the width of the cells is about 20 mm. In the case of the *very* coarse grid II, these grid spacings are 40 mm and 26 mm, respectively. In case of the coarse grid the grid spacing in the center is approximately 12 mm, and in the annular region the width of the cells is about 8 mm. The vertical grid spacing is 100 mm (130 mm) in the case of the *very* coarse grid I (II) and 30 mm in case of the coarse grid. Finally, it has to be emphasized that the transitions between the riser and the solids inlet as well as the riser and the exit pipe were modeled by using mesh interfaces, which do not require coincident meshes of those parts.[40,41]

Bubbling Fluidized Bed

The bubbling fluidized bed consists of a cylinder with 0.267 m inner diameter (compare with Figure 2). This reactor was simulated for comparison with detailed experimental data reported by Zhu et al.[31,42] The height of the reactor was 2.464 m with an added freeboard region expanding to a height of approximately 4.2 m. The freeboard had an inner diameter of 0.667 m to stop excessive particle entrainment out of the bed. The freeboard region was included in the simulation domain to accurately account for the large degree of bed expansion observed in some of the simulations conducted.

Cells were maintained close to perfect cubes in the center, while near the boundaries a boundary layer like structure was employed to better resolve the gradients in wall-normal direction (Figure 2). Two different meshes of the inflow surface (distributor plate) with grid spacings of 1 cm and 2 cm were extrapolated throughout the domain using the cooper meshing method. Consequently, this meshing strategy yields significantly larger elements in the freeboard. However, as the bed did not expand considerably to the freeboard, these larger cells did not affect the final results.

Gas was injected through a velocity inlet on the bottom face of the reactor (Figure 2). Different velocities were employed; on the one hand, we studied $W_g = 0.4$ m s^{-1} and on the other

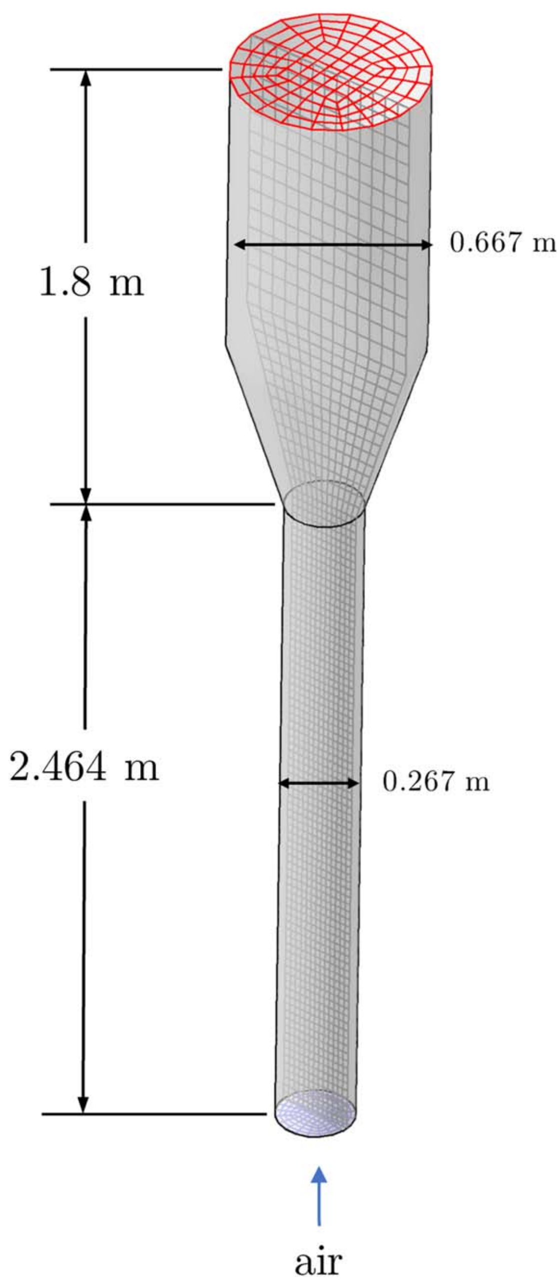

Figure 2. Schematic drawing and mesh of the bubbling fluidized bed.[31,42]

[Color figure can be viewed at wileyonlinelibrary.com] hand, $W_g = 0.9$ m s^{-1}. Gas exited at the top of the reactor though a pressure outlet at 0 Pa gauge pressure. No-slip boundary condition were specified at the walls for both phases (compare with the riser setup). A fine Geldart A powder was used in the bubbling fluidized bed reactor with a density of 1780 kg m^{-3} and a mean diameter of 65 μm.[31] Finally, the particles were agitated by standard air at room temperature.

Results

Riser flow

Our previous study,[43] suggests that the grid resolution for kinetic theory based TFM should be in the order of the characteristic length scale, $\mathbb{L}_{\mathrm{ch}}=(u_t^2/g)\mathrm{Fr}_p^{-2/3}$, where $\mathrm{Fr}=u_t^2/(d_s g)$ is the particle-based Froude number. In particular, this length scale is a good estimate for the size of the smallest clusters, that is where the energy of the clusters dissipates into "molecular" fluctuations. This grid size requirement has also been confirmed recently by others.[44,45] For the group A particles used in this study the characteristic length scale is 220 μm, which is approximately a factor fifty smaller than the horizontal grid spacing of the coarse grid and at least two orders of magnitude smaller than the horizontal grid spacing of the very coarse grids. For the group B particles, the characteristic length scale is 8 mm. However, the contribution stemming from the interparticle collisions (compared to the "turbulent" stresses) can be solely neglected for filter sizes much larger than the above dissipation length scale.[1] Thus, in the case of the coarse grid the interparticle collisions may become non-negligible for the group B particles and the assumptions of the SA-TFM model do not apply. Thus, we only consider the coarse grid in the case of the type A particles and the very coarse grid I for both particle types. To quantify the grid dependency of the SA-TFM approach for the Geldart B type particles we additionally consider the very coarse grid II for Case 5 (Table 1).

Axial pressure profiles

In Figure 3a comparison of the computed time averaged pressure gradients with experimental data (compare with Table 1) is shown. The figure unveils that the dense region at the top of the riser, which is characterized by higher pressure gradients, extends furthest down into the riser for Case 2 using Geldart type A glass beads. This is especially the case for T-shaped exit geometries, where the cavity between riser roof and exit stimulates internal recirculation of particles resulting in increased bed density.[46] However, the Geldart type B particles (Cases 4 and 5) show a much shorter reflux zone at the top. In contrast, Cases 4 and 5 unveil a much longer acceleration and mixing zone than the Geldart A particles at the riser bottom due to their much larger particle relaxation time.

Figure 3a further clearly shows that the SA-TFM model is able to correctly predict solids hold-up in the riser when employing the coarse grid in the case of the Geldart A particles. In particular, the SA-TFM model accurately yields (i) the overall pressure drop (within less than 4%; compare with Table 2), (ii) the dense mixing zone at the solids inlet at the riser bottom, (iii) the widely extended dense reflux zone near the solids outlet at the top of the riser, and (iv) the region of minimum solids concentration in the middle section. Panday et al.[30] further reported that the gas-solid flow for Case 2 is characterized by a dilute upward solids flow in the core and by

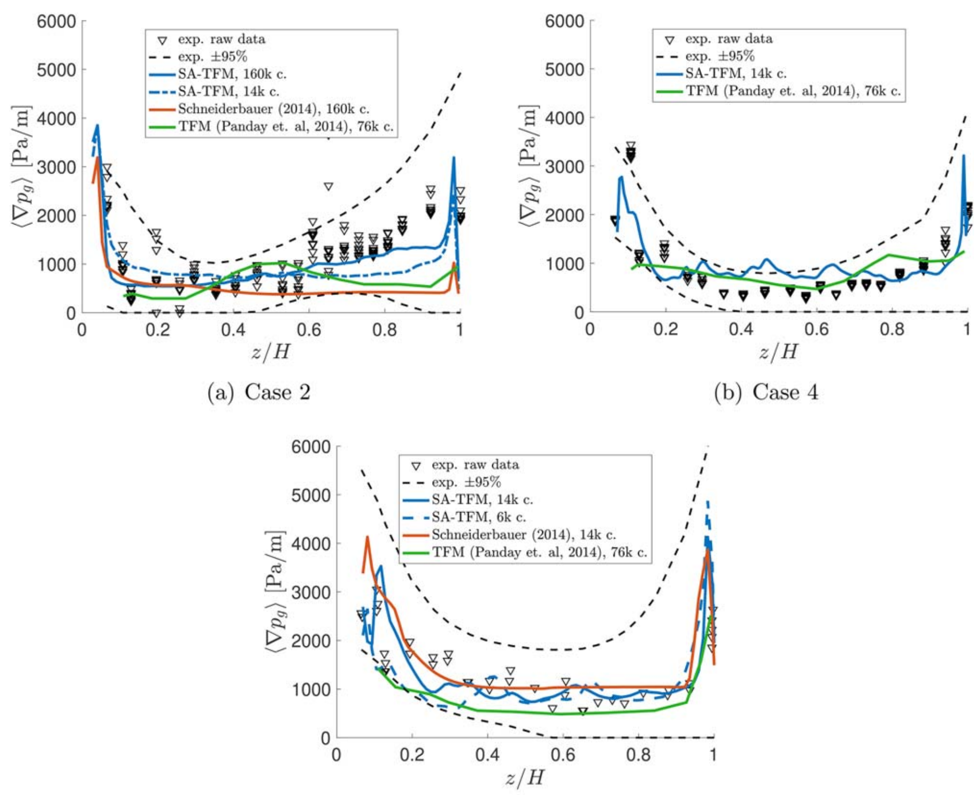

(a) Case 2 (b) Case 4 (c) Case 5

Figure 3. Time averaged pressure gradient, $\langle\nabla p\rangle$, as a function of the normalized vertical coordinate, *z/H*, in the case of riser flow.[30]

[Color figure can be viewed at wileyonlinelibrary.com]

Table 2. Overall Δp in the Case of Riser Flow

	Δp [kPa]			$(\Delta p - \Delta p_e)/\Delta p_e$ [%]		
	Case 2	Case 4	Case 5	Case 2	Case 4	Case 5
Experiment	18.3	13.6	20.9	–	–	–
CG (SA-TFM) [1]	19	–	–	4	–	–
VCG I (SA-TFM) [1]	18.4	15	19.8	0.5	10	5
VCG II (SA-TFM) [1]	–	–	19	–	–	9
CG (filtered TFM) [21]	13	–	–	29	–	–
VCG I(filtered TFM) [21]	–	–	23.9	–	–	10
EE3	8.6	1.9	13.2	53	86	37

CG indicates the coarse grid, VCG the very coarse grids and EE3 the TFM results presented in Panday et al.[30]

dense particle strands at the riser walls, where the particles show nearly no upward velocity or even flow downward (core-annular flow). Those dilute core and dense wall regions are also indicated by Figure 4. Figures 3a and 4 additionally confirm that the SA-TFM model is able to appropriately predict the solids hold-up as well as the core-annular flow even though employing the very coarse grid I. The figures additionally confirm that the present SA-TFM approach is grid independent, as employing the coarse grid and the very coarse grid I unveil nearly identical results. Solely, the distribution of the solids inventory along the riser height slightly differs between both grid resolutions; while the overall pressure drop is nearly equal in both cases (compare with Table 2), the very-coarse-grid-I simulation underestimates the hold-up in the deceleration region near the riser top. This might be due to the very coarse grid resolution, which does not correctly resolve the solid back-mixing due to the T-shaped riser exit.[46]

Figures 3b and 3c present a comparison of the computed pressure gradients for the Geldart type B particles. In both cases, that is, low and high solid recirculation rates, the SA-TFM yields fairly good agreement with the experimental data. Especially, the different behavior near the solids inlet compared to the Geldart A case, that is the more pronounced mixing zone, is accurately determined although we just used 14,000 grid cells (very coarse grid I). Figure 3c further proves the grid independency of the SA-TFM approach in the case of the Geldart type B particles. Employing the very coarse grid II (14,000 grid cells) solely unveils a slightly lower solids inventory in the mixing zone near the solids inlet at the riser bottom, which is discussed later in more detail. Nevertheless, Table 2 confirms that the deviation from the experimental results is less than 10% for both grid resolutions. Similar accuracy was reported by Panday et al.[30] in the case of a TFM simulation with 5,00,000 cells.

We further compared the predictions of the SA-TFM approach with our recently proposed filtered TFM.[21] Similar to the SA-TFM, the latter approach is also based on the Favre-averaged TFM equation. However, in contrast to the SA-TFM approach the constitutive relations for filtered TFM are derived using different markers (in particular, gas voidage and slip velocity) to classify the subfilter scale state. Subsequently, the computational data received from highly resolved simulations is filtered using filters of different sizes and the filtered data is binned and averaged in terms of the values of those markers. Finally, the constitutive relations are directly deduced from those data using curve fitting.[6–8,10,19] Figure 3a unveils that while the filtered TFM approach adequately predicts solids hold-up in the dense mixing zone near the solids inlet in the case of Geldart A particles, it does not yet exhibit the impact of the riser exit. Thus, it considerably underestimate the overall pressure drop by about 29% even though with the coarse grid (CG). Furthermore, Figure 4 clearly indicates that the filtered TFM of Schneiderbauer and Pirker[21] yield a less pronounced dense region near the walls. In particular, the core-annular flow is less pronounced in this case, which results in a lower solids hold-up in the riser. In the case of the Geldart B particles the filtered TFM approach slightly overestimates the pressure gradient by about 10%. A more detailed explanation will be given later.

Finally, Figure 3 demonstrates that using a TFM, which employs a too coarse grid resolution (i.e., 76,000 grid cells), considerably underestimates the solids hold-up in the riser for

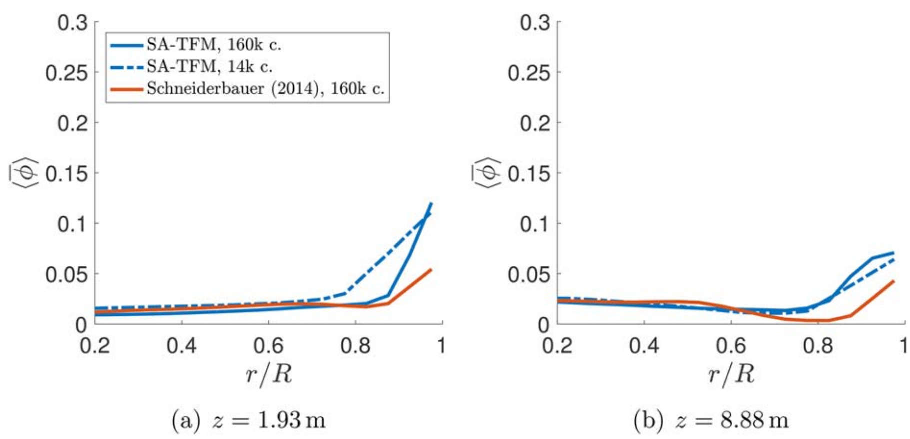

Figure 4. Time averaged solids volume fraction, $\langle\bar{\phi}\rangle$, as a function of the normalized radial coordinate, *r/R*, at different heights for riser flow Case 2.[30]

[Color figure can be viewed at wileyonlinelibrary.com]

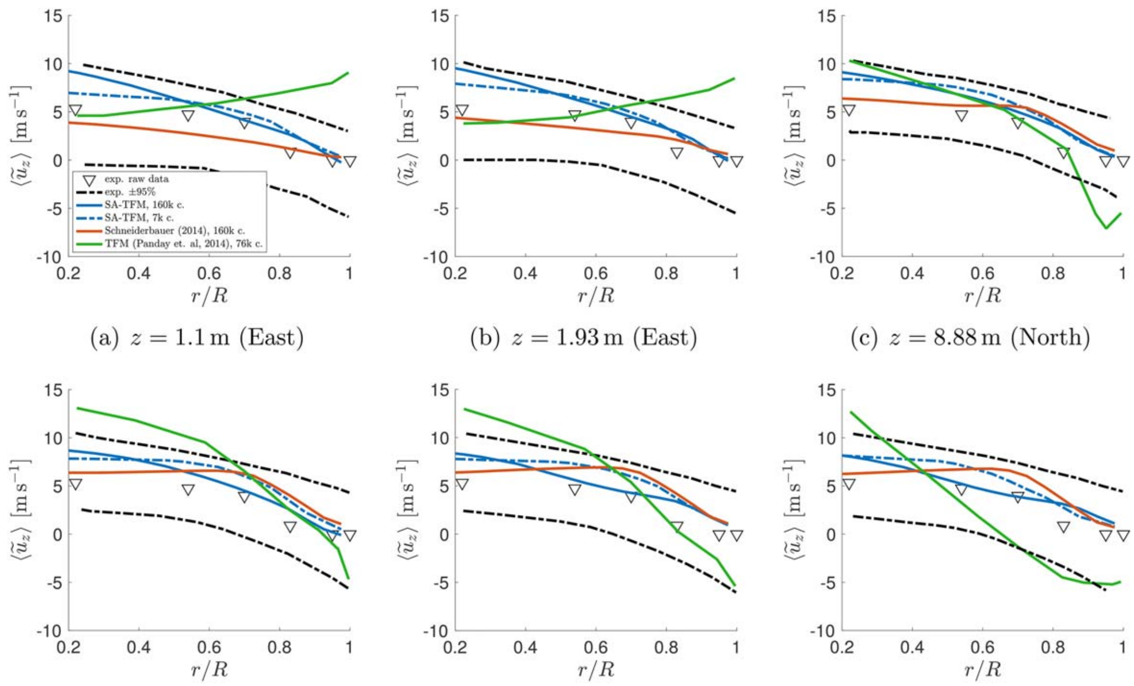

(a) $z = 1.1\,\mathrm{m}$ (East) (b) $z = 1.93\,\mathrm{m}$ (East) (c) $z = 8.88\,\mathrm{m}$ (North)

(d) $z = 13.38\,\mathrm{m}$ (SE-NE) (e) $z = 14.27\,\mathrm{m}$ (East) (f) $z = 15.55\,\mathrm{m}$ (East)

Figure 5. Time averaged vertical solids velocity, $\langle \tilde{u}_z \rangle$, as a function of the normalized radial coordinate, *r/R*, at different heights and azimuthal locations for riser flow Case 2.[30]

The azimuthal locations are defined in Figure 1b. [Color figure can be viewed at wileyonlinelibrary.com]

all cases (compare also with Table 2). Coarse grids inevitably neglect the small (unresolved) scales when using TFM. In particular, TFM requires a grid resolution of approximately u_t^2/g $\mathrm{Fr}^{-2/3}$ to resolve all relevant scales.[43] This length is about 220 μm for the Geldart A particles, which necessitates 10^{12} numerical cells. In the case of the Geldart B particles $u_t^2/g\mathrm{Fr}^{-2/3}$ yields approximately 8 mm, which solely requires 2 million cells. This, in turn, implies that in the case of only 76,000 grid cells the gas-solid drag force is considerably overestimated as the subgrid cluster structure is not accounted for, which yields a substantially smaller pressure drop. However, as mentioned earlier Panday et al.[30] reports that TFM provides appropriate estimates of the solids hold-up for Cases 4 and 5 as long as one uses more than 5,00,000 cells, which is consistent with our estimate of the grid resolution. Nevertheless, using the SA-TFM approach the number of grid cells can be reduced by up to eight orders of magnitude.

Radial solids velocity profiles

The computed radial solids velocity profiles are summarized in Figures 5 through 7. Also shown are the experimental results reported by Panday et al.[30] as well as the 95% confidence intervals of the experiments. Case 2 exhibits a considerable dependence of the solids velocity profiles on the azimuthal location (compare with Figure 1b), Cases 4 and 5 are not significantly different between SE–NW/NE–SW and E–W/N–S directions, where the solids inlet defines the western direction. Thus, Figure 5 reports the radial solids velocity separately for different azimuthal locations and Figures 6 and 7 summarize different directions at a specific height in one plot.

Figure 5 supports the conclusions already drawn from the solid hold-up profiles. The SA-TFM approach is able to capture the shape of the velocity profiles correctly. That is, the vanishing solids velocity near the walls and the high upward velocities in the dilute core (compare also with Figure 4). However, while the computed solids velocities are in good agreement with the experimental data in the wall region, the particle momentum is slightly overestimated in the core. Nevertheless, the presented results lie well within the confidence intervals of the experiments. As there are neither mass flux nor volume fraction measurements available for Case 2 it is impractical to ascertain the reason for this slight mismatch between our results and the experiments. Our simulations might either slightly overestimate the velocity or slightly underestimate the solids volume fraction in the core. The latter, in turn, would directly imply higher solids velocities. Finally, the figure confirms that the solids velocity profiles computed by the SA-TFM approach do not show a considerable grid dependence

In Figures 6 and 7 the radial solids velocity profiles for the Geldart type B particles are presented. The figures clearly demonstrate that the computed solids velocities are in fairly good agreement with the experimental data in the case of the SA-TFM approach. The profiles unveil that the SA-TFM approach appropriately reproduces the low upward solids velocities near the walls as well as identifies the high upward movement of the particles in the center. Especially, Figure 7 confirms the grid independency of the SA-TFM approach in the case of the Geldart B particles. However, for Cases 4 and 5 the solids velocity profiles received from the SA-TFM simulations are significantly flatter than those stemming from the experiments. This may be explained by Figure 8 showing the corresponding time averaged profiles of the solids volume fraction for Case 5. The figure discloses that the simulations yield a very dense annulus region, which is slowly moving upward, and a dilute core region; both regions are clearly

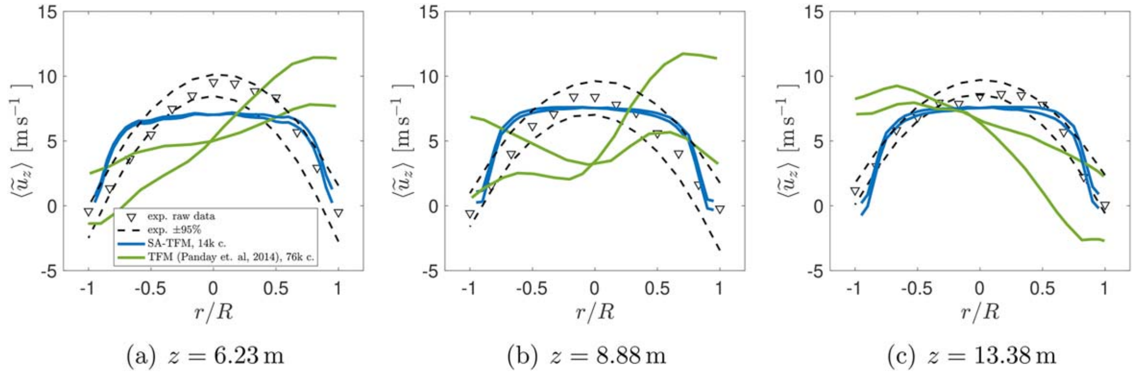

Figure 6. Time averaged vertical solids velocity, $\langle \tilde{u}_z \rangle$, as a function of the normalized radial coordinate, *r/R*, at different heights for riser flow Case 4.[30] The solid lines correspond to two different azimuthal directions, which are: (a) SE–NW and NE–SW; (b) E–W and N–S; (c) E–W and N–S.

The azimuthal locations are defined in Figure 1b. [Color figure can be viewed at wileyonlinelibrary.com]

separated, which is related to the very coarse grid spacings not resolving a smoother transition between both regions. However, as discussed above higher grid resolutions inevitably violates the requirements of the SA-TFM approach in the case of the Geldart type B particles. Additionally, Figure 6 reveals that in the bottom of the riser the center velocity is slightly underestimated in Case 4, which will be discussed later.

Figures 5 through 7 further display the solids velocity profiles received from the filtered TFM of Schneiderbauer and Pirker[21] as well as from TFM reported by Panday et al.[30] While in the case of the Geldart type A particles the solids velocity profiles are in close agreement with the experimental data for the filtered TFM approach, in the case of the Geldart type B particles the solids velocity near the wall is considerably overestimated. This can be associated to the following. One the one hand, Part I[29] of this study clearly demonstrates that state-of-the-art filtered TFM approaches require (i) wall corrections to correctly capture the subgrid state near solid boundaries. Additionally, (ii) the constitutive relations for the Reynolds-stress like contributions do not account for the interfacial work, which considerably impacts the stresses near walls.[29] Particularly, this impacts the solids volume fraction profiles as disclosed by Figures 4 and 8. Conversely, those constitutive relations have been derived by solely considering one particular gas-solid system. Thus, the dependencies on the particle properties as well as fluidization regime on the filtered closures might be included incorrectly. Nevertheless, the filtered TFM approach performs quite well as long as those properties do not show a considerable deviation from its reference system.[21]

Finally, the microscopic TFM appears to correctly predict the shape of the velocity profile in the upper part of the riser while it fails to determine the correct velocity magnitude. In particular, near the walls TFM unveils a considerable downward solids flow and in the center the upward velocity is significantly overestimated. In the bottom of the risers the velocity profile does not even show a vanishing solids velocity when approaching the walls. The highly negative velocities at the bounding walls can be related to the Johnson and Jackson boundary conditions[37] employed in the TFM simulation while the significantly larger velocities in the center are a direct consequence of the overestimation of the interface momentum exchange. Cloete et al.[39] reported that the Johnson and Jackson boundary conditions may strongly over-predict the shear stress and the granular temperature generation at the walls, which results in an unphysical self-strengthening generation of granular temperature in the near-wall regions. This, in turn, has a great impact on the formation of the dense particle strands near the walls, which is reflected in Figure 5. In the case of the Geldart type B particles (Figures 6 and 7) TFM

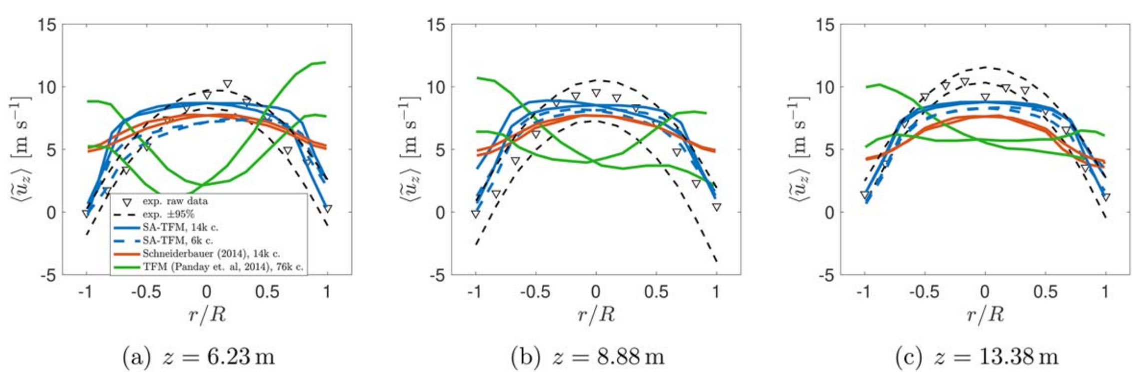

Figure 7. Time averaged vertical solids velocity, $\langle \tilde{u}_z \rangle$, as a function of the normalized radial coordinate, *r/R*, at different heights for riser flow Case 5.[30] The solid lines correspond to two different azimuthal directions, which are: (a) SE–NW and NE–SW; (b) E–W and N–S; (c) E–W and N–S.

The azimuthal locations are defined in Figure 1b. [Color figure can be viewed at wileyonlinelibrary.com]

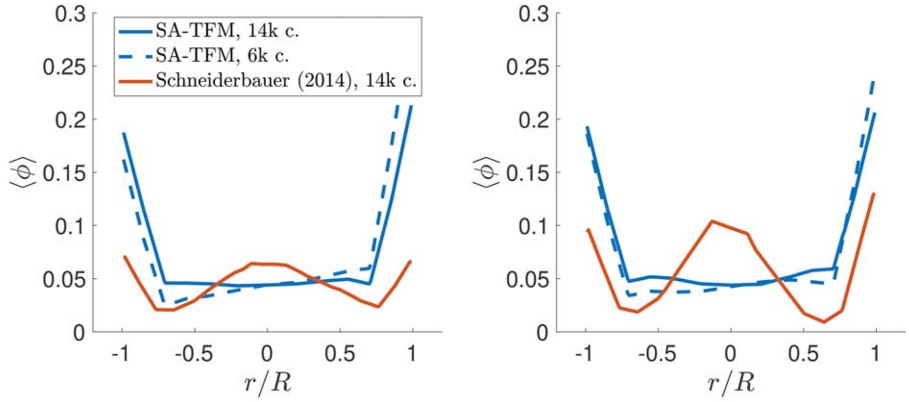

(a) $z = 8.88\,\mathrm{m}$ (b) $z = 13.33\,\mathrm{m}$

Figure 8. Time averaged solids volume fraction, $\langle\bar{\phi}\rangle$, as a function of the normalized radial coordinate, *r/R*, at different heights for riser flow Case 5.[30]

The profiles are plotted along the following azimuthal direction, E–W. The azimuthal locations are defined in Figure 1b. [Color figure can be viewed at wileyonlinelibrary.com]

unveils a completely different behavior than observed from the measurements. Particularly, the solids velocity profiles are highly asymmetric, which indicates that these particular TFM simulations were not converged or have not reached steady state in solids flow.[30] Thus, the asymmetry of the velocity profiles is not a consequence of the modeling methodology of TFM; it may be rather related to a much too short averaging period.

Radial solids mass flux profiles

Figures 9 and 10 show the computed vertical solids mass flux for Cases 4 and 5, respectively. In both cases, the SA-TFM reveals good agreement with the measurements at most locations. Remarkably, the SA-TFM approach appropriately captures the asymmetry of the mass flux profile at 6.23 m elevation observed at Case 5, which is due to high mass flow rate from the solids inlet, when employing the very coarse grid I. However, using even coarser grid resolutions (i.e., very coarse grid II) does not allow to resolve this asymmetry in this case (Figure 10), which yields a lower estimation of the solids inventory in the lower part of the riser. In contrast, the symmetric mass flux profiles in the upper part of the riser are in close agreement with on the one hand, the experiments and on the other hand, the very-coarse-grid-I simulation. Nevertheless, it has to be further emphasized that the present approach also correctly predicts the change of the transport regime between Cases 4 and 5. While Case 4 is characterized by a core-annular flow (nearly zero upward or even negative upward particle flux of the dense strands at the wall), Case 5 is considered as dense suspension flow (which shows non-zero positive particle mass flux at the walls). However, for Case 4 the solids recirculation is slightly overestimated yielding higher vertical solids fluxes in the center, which is due to an overestimation of the solids inventory in the center (compare with Figure 3b). This, in turn, implies that the solids velocity is slightly underestimated in the center (compare with Figure 6). Finally, while the filtered TFM approach unveils the correct magnitude of the solid mass flux (Figure 10), the upward flux near the wall is considerably overestimated, which can be linked to the high positive near wall velocities indicated in Figure 7. Similar to Figures 6 and 7 the coarse grid TFM simulation presented by Panday et al.[30] does not provide an appropriate measure of the particle mass flux. As discussed before, the considerable asymmetry (especially in the top of the riser for Case 4) discloses that these TFM simulations were not converged.

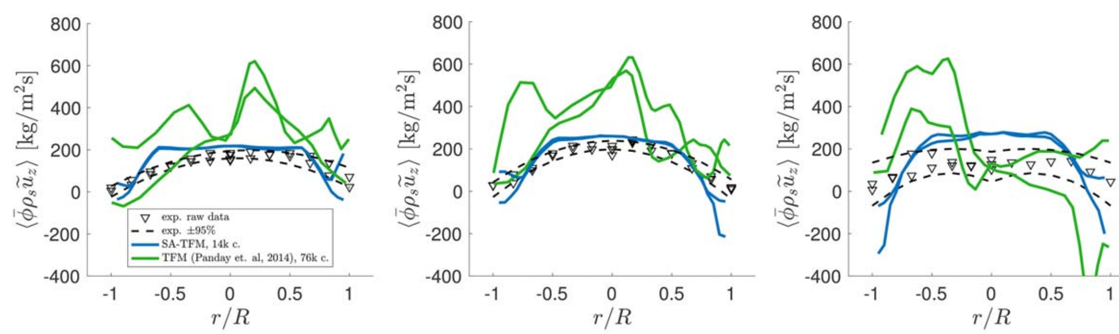

(a) $z = 6.23\,\mathrm{m}$ (b) $z = 8.88\,\mathrm{m}$ (c) $z = 13.33\,\mathrm{m}$

Figure 9. Time averaged vertical solids mass flux, $\langle\bar{\phi}\rho_s\tilde{u}_z\rangle$, as a function of the normalized radial coordinate, *r/R*, at different heights for riser flow Case 4.[30]

The solid lines correspond to two different azimuthal directions, which are: (a) SE–NW and NE–SW; (b) E–W and N–S; (c) E–W and N–S. The azimuthal locations are defined in Figure 1b. [Color figure can be viewed at wileyonlinelibrary.com]

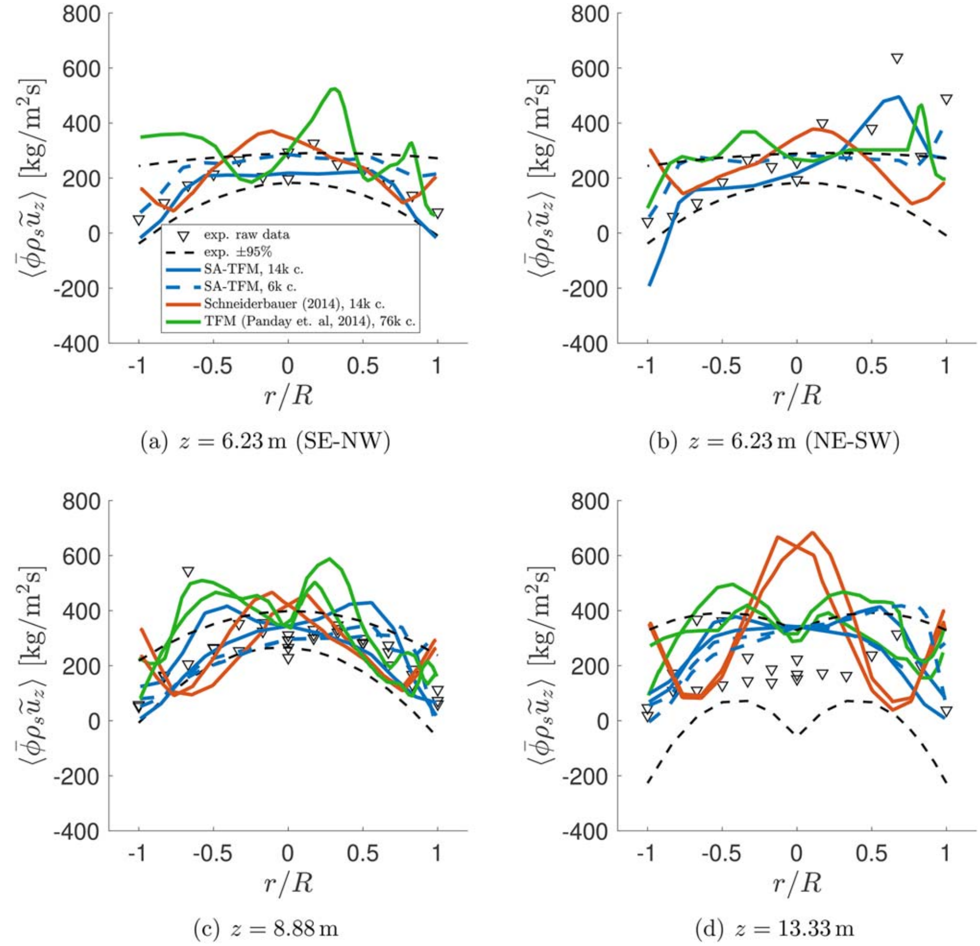

Figure 10. Time averaged vertical solids mass flux, $\langle\bar{\phi}\rho_s\tilde{u}_z\rangle$, as a function of the normalized radial coordinate, *r/R*, at different heights for riser flow Case 5.[30]

The solid lines correspond to two different azimuthal directions, which are: (a) SE–NW and NE–SW; (b) E–W and N–S; (c) E–W and N–S. The azimuthal locations are defined in Figure 1b. [Color figure can be viewed at wileyonlinelibrary.com]

Bubbling fluidized bed

In Figure 11 the time averaged axial pressure gradient for the two different superficial gas velocities is shown. The figure clearly reveals that employing kinetic theory based TFM considerably underestimates the axial pressure gradient as the gas-solid drag force does not account for the unresolved heterogeneous structures. Note that the TFM results are taken from Cloete et al.[47] In contrast, the SA-TFM model correctly predicts the pressure gradient for both superficial gas velocities even though the grid spacing is two orders of magnitude larger than the grid resolution required for TFM. Furthermore,

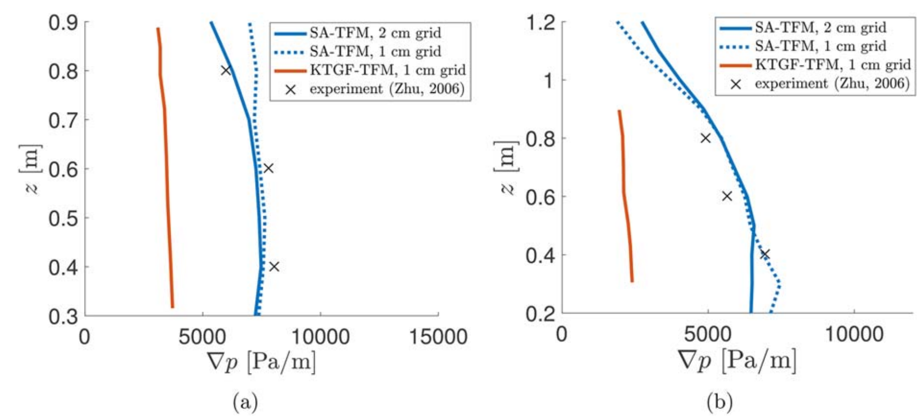

Figure 11. Time averaged pressure gradient, $\langle\nabla p\rangle$, as a function of the normalized radial coordinate, *r/R*, for bubbling fluidized bed[31,42] at $z = 0.6$ m for (a) $W_g = 0.4$ m s^{-1} and (b) $W_g = 0.9$ m s^{-1}.

[Color figure can be viewed at wileyonlinelibrary.com]

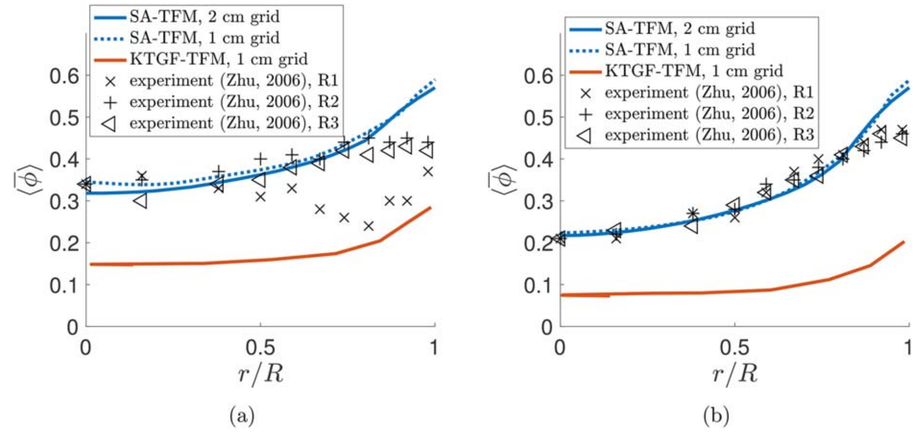

Figure 12. Time averaged solids volume fraction, $\langle\bar{\phi}\rangle$, as a function of the vertical coordinate, z, for bubbling fluidized bed[31,42] at $z = 0.6$ m for (a) $W_g = 0.4$ m s^{-1} and (b) $W_g = 0.9$ m s^{-1}.

[Color figure can be viewed at wileyonlinelibrary.com]

the SA-TFM unveils nearly identical results for grid resolutions of 1 cm and 2 cm und thus, provides grid independent solutions.

Figure 12 shows the time averaged radial solids volume fraction at $z = 0.6$ m. The figure reveals that in the case of vigorous bubbling (i.e., $W_g = 0.4$ m s^{-1}) the model over-predicts the degree of radial solids volume fraction segregation in the vessel. This is observed for both grid resolutions. The particular experimental case with which the simulations are compared exhibited a large degree of nonsymmetry in the flow, even after 30 s of averaging, due to a spiraling bubble motion in the bed.[31,42] This can be seen from the three different time averaged radial measurements (R1, R2, and R3), where one of them differed significantly from the others. This asymmetry is the primary reason for the relatively uniform experimental volume fraction trend shown in Figure 12 and could not be accurately captured by the SA-TFM approach. Similar radial profiles have been obtained by Cloete et al.[47] when employing the filtered closures of Icgi et al.[9] As, spiraling bubble motion is a fairly isolated phenomenon, which may be induced by small asymmetries not present in the simulation, a precise simulation match is therefore not advisable.

In the case of $W_g = 0.9$ m s^{-1} the computed radial segregation is in fairly good agreement with the experiment. Here, the rise of bubbles in the center of the bed induces a recirculation of the solid, where the particles move upward in the center and downward near the wall. As already indicated by Figure 11a kinetic theory based TFM (without accounting for the small unresolved scales) considerably underestimates the solids holdup for both superficial gas velocities.

Figure 13 shows snapshots of the solids volume fraction. The figure clearly unveils that the SA-TFM model reveals is insensitive to the grid resolution with respect to the bed expansion. However, due to grid coarsening one inevitably loses detailed features of the bubbles, which have to be accounted for by the present subgrid corrections. Nevertheless, at both superficial gas velocities distinct bubbles form for both grid resolutions. This is also supported by Figure 14 showing the radial RMS (root means square) profiles of the solids volume fractions. In particular, low RMS values give evidence of less pronounced bubbling of the fluidized bed, while large RMS values indicate distinct bubbling. This, in turn, implies that the bubbling is most pronounced in the center of the bed, while near the wall near no bubbles are present. Furthermore, in both cases our coarse grid simulations yield RMS values, which are in fairly good agreement with the experiment. Thus, the SA-TFM approach reveals a very good measure of the bubbling behavior in fluidized beds. Finally, it has to be noted that the present method does not require wall corrections[7] for the filtered drag and the mesoscale stresses (compare also with Part I of this article). This is in contrast to previous filtered

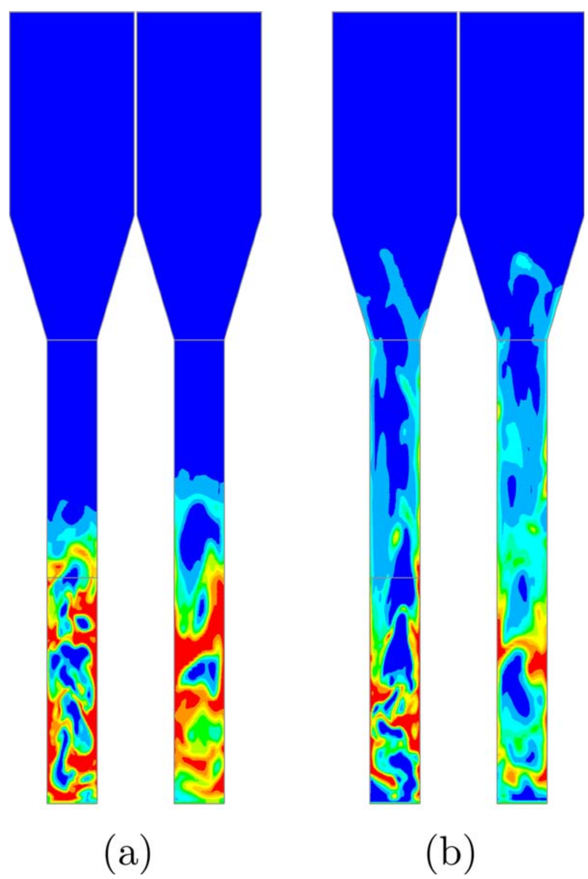

Figure 13. Snapshots of the solids volume fraction for (a) $W_g = 0.4$ m s^{-1} and (b) $W_g = 0.9$ m s^{-1}.

The left figure corresponds to a grid resolution of 1 cm and the right figure to a grid resolution of 2 cm. [Color figure can be viewed at wileyonlinelibrary.com]

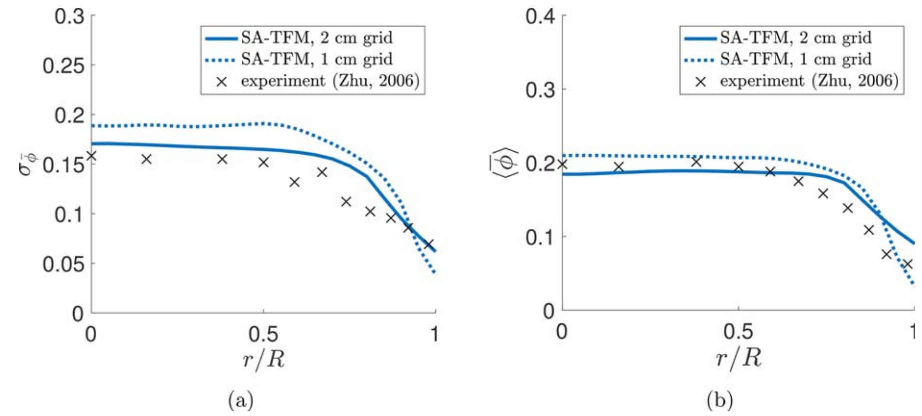

Figure 14. Root means square (RMS) of solids volume fraction, $\sigma\bar{\phi}$, as a function of the vertical coordinate, *z*, for bubbling fluidized bed[31,42] for (a) $W_g = 0.4$ m s^{-1} and (b) $W_g = 0.9$ m s^{-1}.

[Color figure can be viewed at wileyonlinelibrary.com]

TFM approaches,[7] where wall corrections are required to correctly predict the bed expansion in this case.[47]

Conclusions and Outlook

In this article, we applied our previously presented SA-TFM approach[1] to different fluidized bed regimes, such as bubbling and turbulent beds as well as riser flows, utilizing group A and B particles. The SA-TFM approach is based on the turbulent behavior of the heterogeneous gas-solid structures. These appear as additional sources for the turbulent kinetic energies of both phases and for the sub-filter variance of the solids volume fraction due to the interfacial work. Those quantities, in turn, characterize the subgrid heterogeneity and therefore, the unresolved terms in the filtered balance equations can be determined.

First, the results show that applying the SA-TFM approach to the riser flow of group A and B particles yields fairly good agreement with experiments of time average pressure gradient, time averaged vertical particle velocity and time averaged vertical solids mass flux. Furthermore, this model is highly efficient at industrial scale, as we obtained grid independent results up to a grid resolution of 1500 particle diameters in vertical direction in the case of the group A particles. Thus, the SA-TFM approach requires at up to eight orders of magnitude less computational cells than necessary for grid independent kinetic theory based TFM simulations of Geldart A particles. In case of the group B particles such degree of grid coarsening could not be obtained due to geometrical restrictions of the riser. Second the SA-TFM approach applies to bubbling and turbulent beds as well. Here, the time averaged radial profiles of the particle volume fraction and the vertical profiles of the pressure gradient are in good agreement with experimental data up to grid resolutions of 300 particle diameters. Finally, the present method fairly good resolves the larger bubbles, which is supported by an adequate prediction of the RMS values of the solids volume fractions. To sum up, the presented results verify that the SA-TFM approach is applicable to a wide range of particle diameters, different fluidization regimes and to very coarse grid resolutions.

However, the SA-TFM approach is based on the assumption of isotropic mesoscale stresses and an isotropic drag modification, which might not be valid in most gas-solid flows.[19] Thus, future studies will concentration on the extension of the present method to anisotropic stress and drag closures. Additionally, the SA-TFM approach will be further validated against highly resolved simulations of gas-particle flows,[48,49] which exhibit commonly less uncertainty than experimental data. Finally, the current approach will be generalized to heat and mass transfer as well.

Acknowledgments

This work was funded by the Christian-Doppler Research Association, the Austrian Federal Ministry of Economy, Family and Youth, and the Austrian National Foundation for Research, Technology and Development. The author also wants to acknowledge the financial support from the K1MET center for metallurgical research in Austria (www.k1-met.com). Österreichische Forschungsförderungsgesellschaft;Christian Doppler Forschungsgesellschaft.

Literature Cited

1. Schneiderbauer S. A spatially-averaged two-fluid model for dense large-scale gas-solid flows. *AIChE J*. 2017;63(8):3544–3562.
2. Schneiderbauer S, Aigner A, Pirker S. A comprehensive frictional-kinetic model for gas-particle flows: analysis of fluidized and moving bed regimes. *Chem Eng Sci*. 2012;80:279–292.
3. Agrawal K, Loezos PN, Syamlal M, Sundaresan S. The role of meso-scale structures in rapid gas-solid flows. *J Fluid Mech*. 2001; 445:151–185.
4. Lu B, Wang W, Li J. Searching for a mesh-independent sub-grid model for CFD simulation of gas-solid riser flows. *Chem Eng Sci*. 2009;64(15):3437–3447.
5. Wang J, Ge W, Li J. Eulerian simulation of heterogeneous gas-solid flows in CFB risers: EMMS-based sub-grid scale model with a revised cluster description. *Chem Eng Sci*. 2008;63(6):1553–1571.
6. Igci Y, Andrews AT, Sundaresan S, Pannala S, O'Brien T. Filtered two-fluid models for fluidized gas-particle suspensions. *AIChE J*. 2008;54(6):1431–1448.
7. Igci Y, Sundaresan S. Constitutive models for filtered two-fluid models of fluidized gas-particle flows. *Ind Eng Chem Res*. 2011;50(23): 13190–13201.
8. Igci Y, Sundaresan S. Verification of filtered two-fluid models for gas-particle flows in risers. *AIChE J*. 2011;57(10):2691–2707.
9. Igci Y, Pannala S, Benyahia S, Sundaresan S. Validation studies on filtered model equations for gas-particle flows in risers. *Ind Eng Chem Res*. 2012;51(4):2094–2103.
10. Milioli CC, Milioli FE, Holloway W, Agrawal K, Sundaresan S. Filtered two-fluid models of fluidized gas-particle flows: new constitutive relations. *AIChE J*. 2013;59(9):3265–3275.
11. Holloway W, Sundaresan S. Filtered models for reacting gas-particle flows. *Chem Eng Sci*. 2012;82:132–143.
12. Holloway W, Sundaresan S. Filtered models for bidisperse gas-particle flows. *Chem Eng Sci*. 2014;108:67–86.

13. Sarkar A, Sun X, Sundaresan S. Sub-grid drag models for horizontal cylinder arrays immersed in gas-particle multiphase flows. *Chem Eng Sci*. 2013;104:399–412.
14. Parmentier JF, Simonin O, Delsart O. A functional subgrid drift velocity model for filtered drag prediction in dense fluidized bed. *AIChE J*. 2012;58(4):1084–1098.
15. Li J, Kwauk M. *Particle-Fluid Two-Phase Flow: The Energy-Minimization Multi-Scale Method*. Beijing, China: Metallurgical Industry Press, 1994.
16. Wang J, van der Hoef MA, Kuipers JAM. Coarse grid simulation of bed expansion characteristics of industrial-scale gas-solid bubbling fluidized beds. *Chem Eng Sci*. 2010;65(6):2125–2131.
17. Ozel A, Fede P, Simonin O. Development of filtered Euler-Euler two-phase model for circulating fluidised bed: high resolution simulation, formulation and a priori analyses. *Int J Multiphase Flow*. 2013;55:43–63.
18. Radl S, Sundaresan S. A drag model for filtered Euler-Lagrange simulations of clustered gas-particle suspensions. *Chem Eng Sci*. 2014; 117:416–425.
19. Sarkar A, Milioli FE, Ozarkar SS, Li T, Sun X, Sundaresan S. Filtered sub-grid constitutive models for fluidized gas-particle flows constructed from 3-D simulations. *Chem Eng Sci*. 2016;152:443–456.
20. Schneiderbauer S, Puttinger S, Pirker S. Comparative analysis of subgrid drag modifications for dense gas-particle flows in bubbling fluidized beds. *AIChE J*. 2013;59(11):4077–4099.
21. Schneiderbauer S, Pirker S. Filtered and heterogeneity based subgrid modifications for gas-solid drag and solids stresses in bubbling fluidized beds. *AIChE J*. 2014;60(3):839–854.
22. Schneiderbauer S, Saeedipour M. Approximate deconvolution model for the simulation of turbulent gas-solid flows: an a-priori analysis. *Phys Fluids*. 2018;30:23301.
23. Schneiderbauer S, Pirker S. The impact of different fine grid simulations on the sub-grid modification for gas-solid drag. In: Soldati A, Marchioli C, editors. *Proceedings of the 9th International Conference on Multiphase Flow*, Florence, Italy, 2016:6.
24. Cloete JH, Cloete S, Municchi F, Radl S, Amini S. The sensitivity of filtered Two Fluid Models to the underlying resolved simulation setup. *Powder Technol*. 2017;316:265–277.
25. Fox RO. On multiphase turbulence models for collisional fluid-particle flows. *J Fluid Mech*. 2014;742:368–424.
26. Capecelatro J, Desjardins O, Fox RO. On fluid-particle dynamics in fully developed cluster-induced turbulence. *J Fluid Mech*. 2015;780: 578–635.
27. Capecelatro J, Desjardins O, Fox RO. Strongly coupled fluid-particle flows in vertical channels. I. Reynolds- averaged two-phase turbulence statistics. *Phys Fluids*. 2016;28(3):033306.
28. Capecelatro J, Desjardins O, Fox RO. Strongly coupled fluid-particle flows in vertical channels. II. Turbulence modeling. *Phys Fluids*. 2016;28(3):033307.
29. Schneiderbauer S. Validation study on spatially averaged two-fluid model for gas-solid flows: I. A-priori analysis of wall bounded flows. *AIChE J*. In press.
30. Panday R, Shadle LJ, Shahnam M, Cocco R, Issangya A, Spenik JS, Ludlow JC, Gopalan B, Shaffer F, Syamlal M, Guenther C, Reddy Karri SB, Knowlton T. Challenge problem: 1. Model validation of circulating fluidized beds. *Powder Technol*. 2014;258:370–391.
31. Zhu H, Zhu J, Li G, Li F. Detailed measurements of flow structure inside a dense gas-solids fluidized bed. *Powder Technol*. 2008; 180(3):339–349.
32. Smagorinsky J. General circulation experiments with the primitive equations. *Mon Weather Rev*. 1963;91(3):99–164.
33. Schneiderbauer S. Validation study on spatially averaged two-fluid model for dense gas-solid flows. In: Nowak W, Sciazko M, Mirek P. Krakow, editors. *Proceedings of the 12th International Conference on Fluidized Bed Technology*. Poland, 2017:309–316.
34. Shur ML, Spalart PR, Strelets MK, Travin AK. A hybrid RANS-LES approach with delayed-DES and wall-modelled LES capabilities. *Int J Heat Fluid Flow*. 2008;29(6):1638–1649.
35. Schneiderbauer S, Puttinger S, Pirker S, Aguayo P, Kanellopoulos V. CFD modeling and simulation of industrial scale olefin polymerization fluidized bed reactors. *Chem Eng J*. 2015;264:99–112.
36. Wen CY, Yu YH. Mechanics of fluidization. *Chem Eng Prog Symp Ser*. 1966;62:100.
37. Johnson PC, Jackson R. Frictional-collisional constitutive relations for granular materials, with application to plane shearing. *J Fluid Mech*. 1987;176(1):67–93.
38. Schneiderbauer S, Schellander D, Löderer A, Pirker S. Non-steady state boundary conditions for collisional granular flows at flat frictional moving walls. *Int J Multiphase Flow*. 2012;43:149–156.
39. Cloete JH, Cloete S, Radl S, Amini S. Evaluation of wall friction models for riser flow. *Powder Technol*. 2016;303:156–167.
40. ANSYS. *ANSYS FLUENT Theory Guide*. Vol. 15317. Canonsburg, PA: ANSYS, 2011.
41. ANSYS. *ANSYS FLUENT User's Guide*. *Vol*. 15317. Canonsburg, PA: ANSYS, 2011.
42. Zhu H. Turbulent fluidized bed vs. high density riser - regimes and flow characterizations. Phd thesis, The University of Western Ontario. 2006.
43. Sundaresan S, Radl S, Milioli CC, Milioli FE. Coarse-grained models for momentum, energy and species transport in gas-particle flows. In: Kuipers JAM, Mudde RF, van Ommen JR, Deen NG, editors. *The 14th International Conference on Fluidization - From Fundamentals to Products, ECI Symposium Series*. Noordwijkerhout, The Netherlands: Engineering Conferences International, 2013;8.
44. Fullmer WD, Hrenya CM. The clustering instability in rapid granular and gas-solid flows Granular medium: solid particles in the absence of an interstitial (carrier) phase or in the presence of a negligible gas phase. *Annu Rev Fluid Mech*. 2017;49:485–510.
45. Uddin MH, Coronella CJ. Effects of grid size on predictions of bed expansion in bubbling fluidized beds of Geldart B particles: a generalized rule for a grid-independent solution of TFM simulations. *Particuology*. 2017;34:61–69.
46. Shadle L. The effect of riser end geometry on gas-solid hydrodynamics in a CFB riser operating above fast fluidization regimes. In: Chaouki J, Cocco R, editors. *FLUIDIZATION XV*, Fairmont Le Chateau Montebello, Quebec, Canada: ECI Symposium Series, 2016.
47. Cloete S, Johansen ST, Amini S. Evaluation of a filtered model for the simulation of large scale bubbling and turbulent fluidized beds. *Powder Technol*. 2013;235:91–102.
48. Kong B, Fox RO, Feng H, Capecelatro J, Patel R, Desjardins O, Fox RO. Euler-Euler anisotropic Gaussian mesoscale simulation of homogeneous cluster-induced gas-particle turbulence. *AIChE J*. 2017;63(7):2630–2643.
49. Patel RG, Kong B, Capecelatro J, Desjardins O, Fox RO. Verification of Eulerian-Eulerian and Eulerian-Lagrangian simulations for turbulent fluid-particle flow. *AIChE J*. 2017;63(12):5396–5412.
50. Cloete S, Johansen ST, Amini S. Grid independence behaviour of fluidized bed reactor simulations using the Two Fluid Model: effect of particle size. *Powder Technol*. 2015;269:153–165.

Manuscript received Nov. 7, 2017, and revision received Jan. 18, 2018.